Trans. JSASS Aerospace Tech. Japan
Vol. 10, No. ists28, pp. Tb_17-Tb_23, 2012

Topics

Study on Helicon Plasma Lissajous Acceleration for Electrodeless Electric Propulsion

By Takahiro NAKAMURA[1)], Kenji YOKOI[1)], Hiroyuki NISHIDA[1)], Takeshi MATSUOKA[2)], Ikkoh FUNAKI[2)] Shunjirou SHINOHARA[1)], Takao TANIKAWA[3)], Tohru HADA[4)], Taisei MOTOMURA[4)], Konstantin P. SHAMRAI[5)] and Timofei S. RUDENKO[5)]

[1)] *Department of Mechanical Systems Engineering, Tokyo University of Agriculture and Technology, Koganei, Japan*
[2)] *The Institute of Space and Astronautical Science, JAXA, Sagamihara, Japan*
[3)] *Research Institute of Science and Technology, Tokai University, Hiratsuka, Japan*
[4)] *Interdisciplinary Graduate School of Engineering Sciences, Kyushu University, Kasuga, Japan*
[5)] *Institute for Nuclear Research, National Academy of Sciences of Ukraine, Prospect Nauki, Ukraine*

(Received June 27th, 2011)

In order to realize a long lifetime of an electric propulsion system, we have been investigating various electrodeless electric propulsion concepts utilizing a helicon plasma source. In one of our concepts, helicon plasma is electromagnetically accelerated using a rotating electric field in the presence of a diverging static magnetic field. This acceleration concept is called the Lissajous acceleration. Plasma acceleration experiments have been conducted and plasma acceleration was evaluated using a Mach probe. Although the experiments showed some features of the electromagnetic acceleration, most increment of the plasma velocity is caused by the increment of the electron temperature. The thrust (4.95 μN) did not reach feasible values for real applications, and therefore, it is important to find a better operational condition with the aid of a theoretical thrust model. We have developed a theoretical thrust model which consists of a trajectory analysis and an electric field penetration model in the electrostatic approximation. The model shows that experimental parameters are off from an optimum operational condition which provides the maximum thrust.

Key Words: Electrodeless Plasma Thruster, Rotating Electric Field, Lissajous Acceleration, Helicon Plasma

Nomenclature

a	:	magnetic coil radius
$\mathbf{B}$	:	magnetic flux density vector
C_S	:	acoustic velocity
C, D	:	initial position of particle
$\mathbf{E}$	:	electric field vector
e	:	electron charge
F	:	thrust force
J	:	ion saturation current
k_B	:	Boltzman constant
M_i	:	ion acoustic Mach number
m	:	particle mass
n	:	number density
L	:	axial length of acceleration area
q	:	charge of particle
r	:	radial distance
r_0	:	cross sectional radius of thruster
R_L	:	Larmor radius
R_D	:	**E**x**B** drift gyration radius
T	:	temperature
t	:	time
$\mathbf{v}$	:	velocity
V	:	amplitude of the REF voltage
x, y, z	:	coordinate
α	:	initial direction of thermal velocity
β	:	reduction rate of plasma density
ε	:	angular frequency ratio
κ	:	coefficient for para-perp type Mach probe
μ	:	dimensionless parameter
ω	:	angular frequency of REF
ω_c	:	angular frequency of cyclotron motion
ω_p	:	plasma frequency

Subscripts

e	:	electron particle
i	:	ion particle
x, y, z	:	component
0	:	initial

1. Introduction

An electric propulsion system is suitable for long-time space missions such as interplanetary flights and satellite attitude control. The Japanese asteroid explorer “Hayabusa” has four ion engines which are one of electric propulsion systems, and the mission was successfully accomplished. However, conventional electric propulsion systems have some problems about the lifetime due to electrode erosion and contamination caused by contacts between electrodes and the

plasma.

The electrodeless plasma thruster, in which the electrodes do not contact with the plasma, is one of solutions for these problems [1]. Some of typical examples of electrodeless plasma thruster adopt the electro-thermal plasma acceleration {Variable Specific Impulse Magnetoplasma Rocket (VASIMR) [2]} or electro-static plasma acceleration {Helicon Double Layer Thruster (HDLT) [3,4]}. The plasma source of these thrusters is based on the helicon plasma discharge. The helicon plasma source is one of the radio frequency (RF) plasma production methods which are an electrodeless plasma source. In VASIMR, the plasma is heated by ion cyclotron resonance and subsequently accelerated in a magnetic nozzle. In HDLT, the plasma is accelerated by the electrical potential gap between high density plasma inside the source region and low density plasma in the exhaust. On the other hand, the electromagnetic plasma acceleration is expected to achieve a higher performance than the electro-thermal plasma acceleration [5-7]. In this study, we focus on the electrodeless electromagnetic plasma acceleration.

In order to develop the electrodeless electromagnetic plasma thruster, we have initiated the HEAT (Helicon Electrodeless Advanced Thruster) project in Japan and have been investigating various concepts utilizing a helicon plasma source [8-10]. In the HEAT project, three types of electrodeless electromagnetic plasma acceleration concept have been investigated: Lissajous acceleration, rotating magnetic field (RMF) acceleration and ion acceleration by the use of ponderomotive force as shown in Fig. 1.

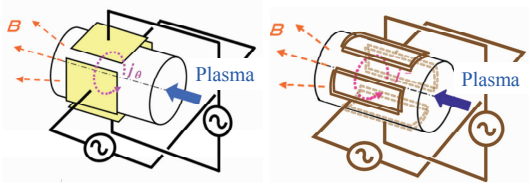

(a) Lissajous acceleration (b) RMF acceleration

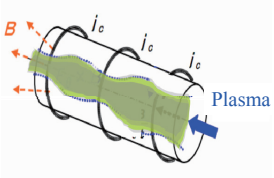

(c) Ponderomotive force acceleration

Fig. 1. Three types of electrodeless electromagnetic plasma acceleration.

In this paper, electromagnetic plasma acceleration by a rotating electric field (REF) called as Lissajous acceleration is discussed. Figure 2 shows the configuration of the Lissajous acceleration type thruster. The thruster consists of a plasma production part and a plasma acceleration part. In the plasma production part, a compact helicon plasma source produces high density plasma by applying an RF power under a static magnetic field. In the acceleration area which lies downstream of the helicon plasma source, a rotating electric field (REF) in the radial direction of the thruster is applied to the plasma by the two pairs of deflection plates in order to induce an azimuthal electron current. Here radial direction is in the *x*-*y* plane in Fig. 2 and the *z* direction is refereed as the axial direction. The Lorentz force, which is a product of the azimuthal electron current and the radial magnetic field, accelerates the helicon plasma in the axial direction. This acceleration method is called as the Lissajous acceleration. The entire process in this thruster can be conducted without contacts between electrodes and the plasma.

In our previous works, high density helicon plasma up to 10^{19} m^{-3} has been successfully produced in the glass tube of 25 mm inner diameter (I.D.) [11-13] and some plasma acceleration were observed when the REF was applied to the plasma [14,15]. In order to find a parameter range where Lissajous acceleration dominates other acceleration processes such as the electron thermal acceleration, an analytical thrust model is developed [15,16] which requires radial profiles of plasma parameters as an input. Therefore, it is important to obtain the detailed spatial distribution of the plasma plume and an evaluation of thrust by use of the plasma parameters obtained in experiments.

In this paper, detailed measurements of the plasma plume by use of a Mach probe and an evaluation of the thrust based on the experimental parameters are reported. Thrust force is evaluated from the experimentally observed plasma parameters and is compared with the force estimated by the theoretical thrust model. Some guidelines for improving the thrust performance based on a theoretical thrust model.

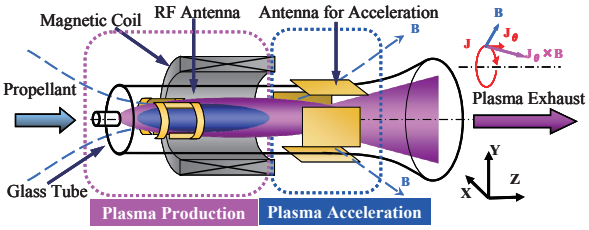

Fig. 2. Schematic of Lissajous acceleration thruster.

2. Principle of the Lissajous Acceleration

The principle of Lissajous acceleration is briefly explained using a two-dimensional electron trajectory analysis. Here, we consider the two-dimensional motion of an electron on the cross-sectional plane (*x*-*y* plane) in the acceleration area. The REF lies in the *x*-*y* plane. A uniform static magnetic field is assumed to be in the *z* direction. The motion equation of a charged particle under the electric field and the magnetic field in above mentioned geometry can be written as,

$$m_e \frac{d\mathbf{v}_e}{dt} = q\left(\mathbf{E} + \mathbf{v}_e \times \mathbf{B}\right). \tag{1}$$

The REF and the magnetic field are represented by following equations and are substituted to Eq. (1).

$$\mathbf{E} = \begin{pmatrix} E_0 \cos(\omega t) \\ E_0 \sin(\omega t) \\ 0 \end{pmatrix}, \tag{2}$$

$$\mathbf{B} = \left(0, 0, B_z\right). \tag{3}$$

Solutions of velocities are obtained as follows,

$$\begin{pmatrix} v_x \\ v_y \end{pmatrix} = \begin{pmatrix} v_0 \cos(-\omega_{ce}t+\alpha) - \dfrac{eE_0}{m_e\omega}\dfrac{1}{-\omega_{ce}/\omega+1}\sin(\omega t) \\ -v_0 \sin(-\omega_{ce}t+\alpha) + \dfrac{eE_0}{m_e\omega}\dfrac{1}{-\omega_{ce}/\omega+1}\cos(\omega t) \end{pmatrix}. \quad (4)$$

The trajectory of the electron can be obtained by integrating Eq. (4).

$$\begin{pmatrix} x \\ y \end{pmatrix} = \begin{pmatrix} -\dfrac{v_0}{\omega_{ce}}\sin(-\omega_{ce}t+\alpha) \\ \quad + \dfrac{eE_0}{m_e\omega^2}\dfrac{1}{-\omega_{ce}/\omega+1}\cos(\omega t) + C \\ -\dfrac{v_0}{\omega_{ce}}\cos(-\omega_{ce}t+\alpha) \\ \quad + \dfrac{eE_0}{m_e\omega^2}\dfrac{1}{-\omega_{ce}/\omega+1}\sin(\omega t) + D \end{pmatrix}. \quad (5)$$

The first term in the right hand side of Eq. (5) expresses the cyclotron motion and the second term expresses the motion due to the REF. The particle rotates around the magnetic field by the REF. When the frequency of the REF ω is chosen to be much higher than the lower hybrid frequency and much lower than the electron cyclotron frequency, the Larmor radius and the gyration radius by the REF are given for the electron as follows:

$$R_L = \frac{v_0}{\omega_{ce}}, \quad R_D = \frac{E_0}{B_z\omega}. \quad (6)$$

Figure 3 (a) shows the trajectory of the electron in the case of R_L/R_D = 0.11 and ω_{ce}/ω = 28. As shown in Fig. 3 (a), the trajectory of the electron is superposition of the small cyclotron gyration and the large **ExB** drift gyration.

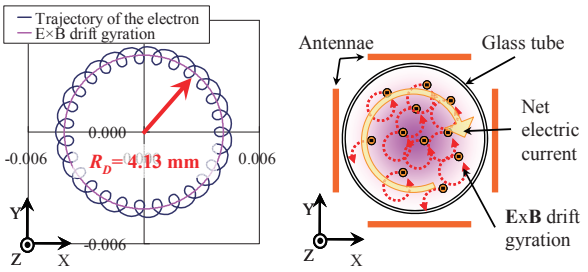

Fig. 3. (a) Trajectory of the electron under REF and uniform magnetic field: R_L/R_D = 0.11 and ω_{ce}/ω = 28. (b) Induction of azimuthal electric current by superposition of the **ExB** gyration motions.

Generation mechanism of the azimuthal electron current in this thruster is different from that in the Hall-effect thruster. In this thruster, **ExB** drift gyro radius R_D is much smaller than the thruster radius. The azimuthal electric current, which is indispensable source for the electromagnetic acceleration, can be produced by superposition of the **ExB** gyration motions of all electrons as shown in Fig. 3 (b). A radial density gradient is important for producing the azimuthal electric current. When the plasma density is uniform, the total current should be zero because each current is canceled by a neighboring electron motion. The theoretical thrust model of the Lissajous acceleration has been proposed by using the two-dimensional electron trajectory analysis and a one-dimensional RF sheath model in the electrostatic field assumption [16]. The induced azimuthal electric current density j_θ [A/m^2] can be obtained as Eq. (7) by integrating individual electron trajectories for an axial symmetric density profile. The theoretical thrust force F [N] is obtained as Eq. (8) by spatial integration of $j_\theta(r)$x$B_r(r)$ with $B_r(r) = B_Z \cdot r/2a$ in the acceleration area. Eq. (7) and (8) are represented under following assumptions: $R_L << R_D << r_0$, $v_i << v_e$ and the plasma density distribution $n(r) = n_0(1-\beta r^2/r_0^2)$.

$$j_\theta = -\frac{2}{3}e\beta n_0\left(\frac{v_D R_D}{r_0} + \frac{v_0 R_L}{r_0}\right), \quad (7)$$

$$F = \frac{\pi}{4}e\beta n_0 L\frac{r_0^2}{a}\left(\frac{E_{p0}^2}{\omega B_z} + \frac{v_0 m_e}{e}\right). \quad (8)$$

Here, the amplitude of the REF penetration into a uniform magnetized plasma (E_{p0}) is obtained from a 1D analysis [16] and is given by,

$$E_{p0}\Big/\frac{V_0}{2r_0} = 1 - \frac{1}{\mu}\left[\varepsilon - \sqrt{\varepsilon^2+\mu}\right]^2, \quad (9)$$

$$\varepsilon = 1 - \frac{\omega^2}{\omega_{ce}^2} \approx 1, \mu = \frac{2eV_0\omega_{pe0}^2}{m_e r_0^2 \omega_{ce}^4}. \quad (10)$$

In this theoretical thrust model, collision-less plasma is assumed, and so the Hall parameter is enough large. However, when the collision cannot be negligible, the **ExB** drift radius R_D becomes smaller than the Eq. (6) because of particle collision [12]. As a result of the R_D reduction, the thrust decreases with increasing the particle collision.

3. Experiment of Lissajous Acceleration

Experiments of Lissajous plasma acceleration are conducted in order to obtain radial profiles of the electron temperature and plasma velocity of the plume for evaluating the plasma acceleration.

3.1. Experimental setup and procedures

A 26 mm I.D. with totally 400 mm long glass tube is connected to a vacuum chamber (Fig. 4). The setup of the plasma production part and the plasma acceleration part is shown in Fig. 5. Ar gas is supplied from a metallic end plate with a gas port into the glass tube. Two power supplies provide RF power for plasma production and acceleration independently. A saddle type antenna is used for the plasma production and two pairs of deflection plates are used for the plasma acceleration. A coil which surrounds the glass tube applies magnetic fields up to 0.145 T at the center of the coil.

The vacuum pump evacuated the chamber down to 10^{-3} Pa or lower, and the Ar gas is fed by a mass flow controller at a predetermined mass flow rate of 0.5 mg/s which is corresponding to the background pressure of 8.2x10^{-2} Pa. A signal generator and a 500 W RF amplifier with a matching box at the frequency of 27.12 MHz are used for the plasma production. For plasma acceleration, two RF signals, which are fed from a function generator, are sent to a phase shifter in

order to adjust the relative phase (δ) between those two RF signals and subsequently amplified by two 200 W amplifiers. The frequency range of the amplifiers is between 20 and 60 MHz. Each amplified signal is sent to a set of deflection plates through a matching box. Acceleration antennae consist of two pairs of deflection plate and each plate is 50 mm long and 20 mm width.

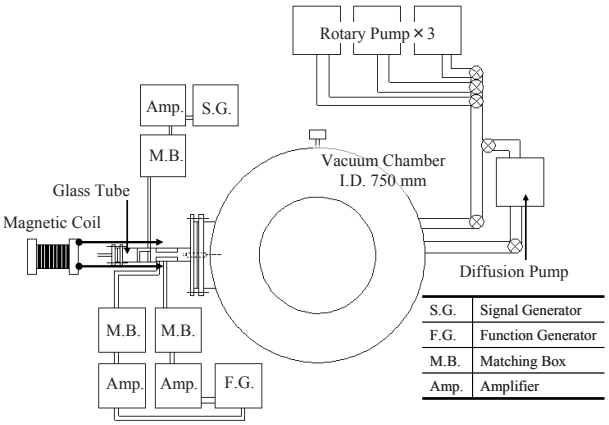

Fig. 4. Experimental facility.

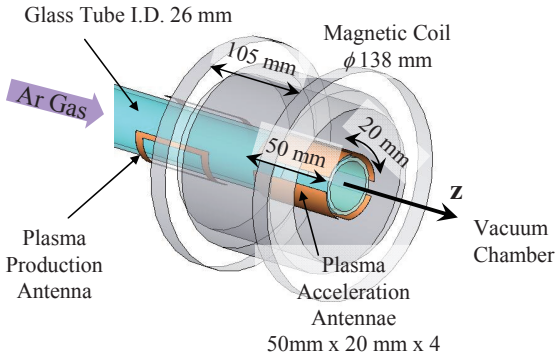

Fig. 5. Enlarged view of the thruster.

A para-perp type Mach probe is used for measuring the ion acoustic Mach number, the electron temperature and plasma density [17]. The Mach probe has two directional tips, which are facing parallel and perpendicular to the plasma flow respectively, as shown in Fig. 6.

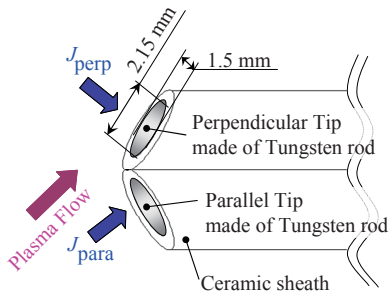

Fig. 6. para-perp type Mach probe.

Ion acoustic Mach number can be obtained by measuring the parallel and perpendicular directional ion saturation currents to the plasma flow. The ion acoustic Mach number M_i is expressed in Eq. (11) and (12) as the ratio of ion saturation currents. Here, coefficient κ is dependent on the ratio of T_i/T_e.

$$\frac{J_{para}}{J_{perp}} = \frac{M_i}{\kappa} \quad (M_i > 1) . \tag{11}$$

$$\frac{J_{para}}{J_{perp}} = \exp\left(aM_i^{1/a}\right), \quad a = -\ln\kappa \quad (M_i < 1) . \tag{12}$$

Electron temperature and electron density can be also measured by using the Mach probe as a double probe. The plasma velocity is obtained from Eq. (13).

$$v = M_i \cdot C_s = M_i \cdot \sqrt{\frac{k_B(T_e + T_i)}{m_i}} . \tag{13}$$

Ion temperature is fixed at the 0.3eV, which is a typical temperature of helicon plasma. Since the plasma acoustic velocity is dominated by the electron temperature, the assumption of the constant ion temperature is expected to be validated.

Experiments are conducted by varying the relative phase (δ). The direction of the electric field oscillation is changed by varying the phase difference as shown in Fig. 7 and the direction of the electromagnetic force is also changed by changing the rotating direction of the electric field. If the electromagnetic force is acting on the plasma, the plasma is accelerated or decelerated depending on the phase difference. The plasma is accelerated (decelerated) at δ = 90° (-90°).

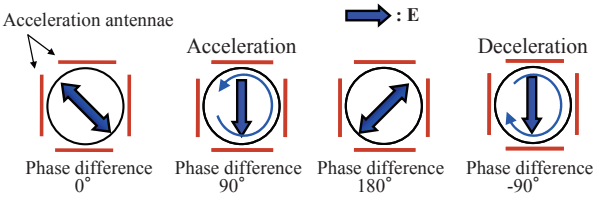

Fig. 7. Applied electric field varying the phase difference between two pairs of the antennae (views from downstream end).

3.2. Experimental conditions

Experimental conditions are shown in Table 1.

Table 1. Experimental conditions.

Vacuum pressure	8.2×10^{-2} Pa
Mass flow rate of Ar gas	0.5 mg/s
Axial magnetic field intensity	0.0950 T
Plasma production power	290 W
Plasma acceleration power	125 W
REF frequency	27.12 MHz

3.3. Experimental results

Figures 8 (a), (b), (c) and (d) show the Mach number, electron temperature, plasma density, and plasma velocity plotted against the phase difference, respectively. The plasma parameter is measured 20 mm downstream from the end of the acceleration antennae and at r = 0 mm. Results before applying the acceleration power are shown with the dashed line and this level is refereed as the base in this paper. A weak dependency on the phase difference can be observed in the Mach number by the slight increase in the range of the phase difference from 0 degree to 90 degrees as shown in Fig. 8 (a). The increase of the plasma velocity is observed in a wide range of δ in a range except for the vicinity of -90° and shows

a peak increments of 1,000 m/s at the phase difference of approximately 90° from the base as shown in Fig. 8 (d). Similar increment is observed for the electron temperature as shown in Fig. 8 (b).

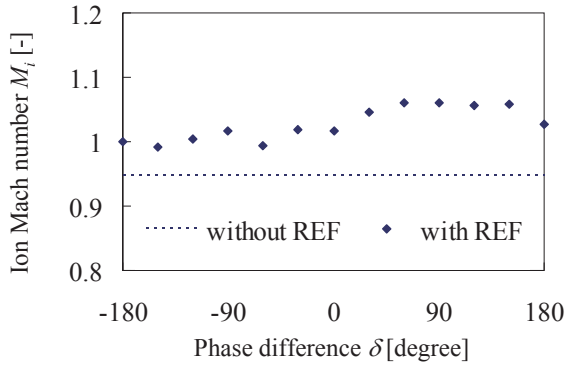

(a) Mach number

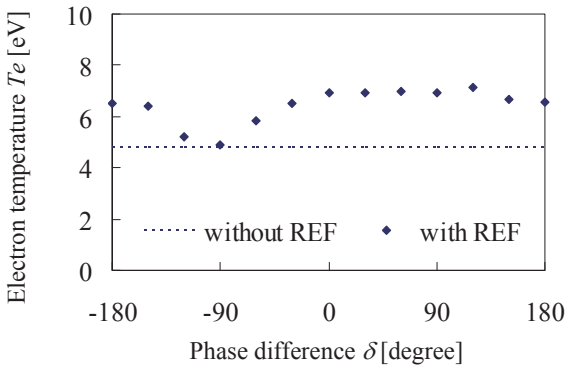

(b) Electron temperature

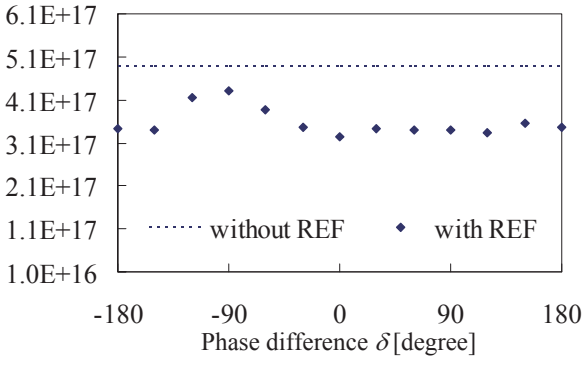

(c) Electron density

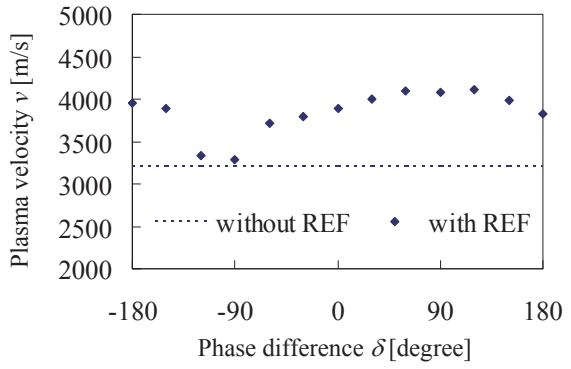

(d) Plasma velocity

Fig. 8. Experimental results varying the phase difference.

When the plasma is accelerated by the Lorentz force between radial magnetic field and azimuthal electric current, the electron temperature should not change in the case of collision-less plasma, or be reduced by the adiabatic expansion. Therefore, if the Lorentz force is only acting on the plasma, the ion Mach number is expected to significantly increase with increasing the plasma velocity. Except in the vicinity of -90°, significant dependence of the Mach number on the phase difference cannot be observed; this result indicates weak electromagnetic acceleration of the plasma. When the phase difference is equal to -90°, the plasma condition does not changed by the REF power, and this result indicates that the electrical power from the power supply is not absorbed by the plasma. In addition, the trend of the change in the plasma velocity with the phase difference is strongly correlated with the change in the electron temperature. Therefore, it is considered that almost of the power for the plasma acceleration is consumed for heating the plasma and the plasma acceleration is mainly due to the thermal effect.

The radial distribution of the plasma parameter is measured 50 mm downstream from the end of the acceleration antennae for the case of the phase difference of 120°, at which the maximum velocity is achieved. The radial distribution of the plasma velocity and the plasma density are shown in Figs. 9 and 10, respectively.

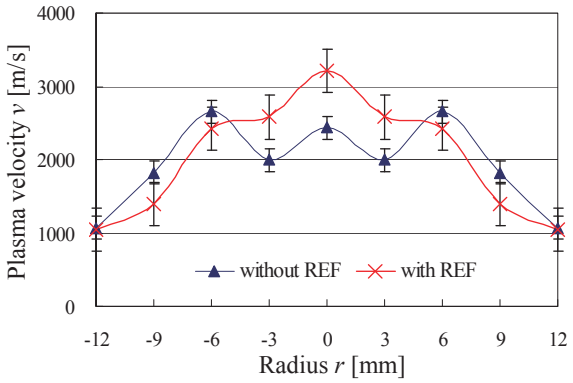

Fig. 9. Plasma velocity distribution. Phase difference δ = 120° and measurement position z = 50 mm downstream form the end of the acceleration antennae.

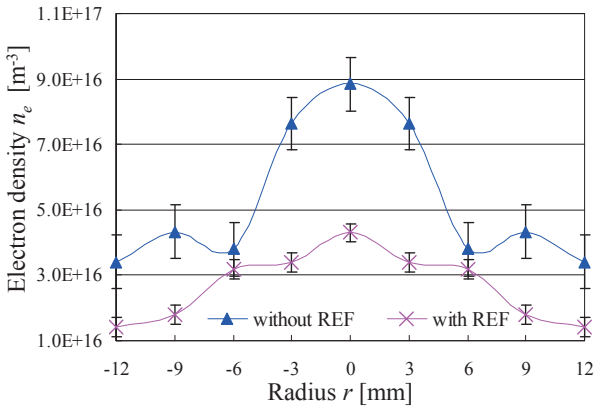

Fig. 10. Plasma density distribution. Phase difference δ = 120° and measurement position z = 50 mm downstream form the end of the acceleration antennae.

The plasma acceleration by applying the REF can be confirmed in these figures. The electron density with the REF is lower than the base due to acceleration of the plasma.

Eq. (14) shows the thrust force evaluated from integrating the momentum flux obtained from the experiments, and the evaluated thrust is 4.95 μN.

$$F = \int_0^{r_0} n_{(r)} v_{(r)}{}^2 m_{ion} \cdot 2\pi r \cdot dr \,. \tag{14}$$

Contribution from neutral flow is not included thus the thrust is underestimated compared with actual thrust. The fitted curve to the density distribution shown in Fig. 10 reveals that the reduction rate of the plasma density β (in Eqs. (7) and (8)) is 0.685. The thrust is theoretically estimated to be 14.2 μN by substituting the β and experimental other geometrical parameters to the theoretical thrust Eq. (7). The experimental thrust is smaller than the theoretical estimation. From previous experiment, the plasma density inside the acceleration area is approximately 50 times denser than the density at the measurement point. Using the density inside of the acceleration area, the estimated thrust is greater than the experimental thrust by a factor of 200. Therefore the validity of the model may not be confirmed by the data shown here. The discrepancy could arise due to lack of key physics such as wall particle loss, collisions and non-uniformity of the parameters in the theoretical thrust model. The experimental uncertainty could also be a reason in particular to the RF voltage applied on the antennae and nun-uniformity of the REF. Voltage of applied REF is taken from values of matching boxes. Experiments are planned to measure the RF voltage.

4. Discussions for Enhancing Thrust Force

As it is discussed in the previous section, the theoretical thrust model is under development. We plan to benchmark the model by selecting parameter sets for future experiments such that the thrust model shows maximum electromagnetic force. The theoretical thrust distributions in the parameter planes of the axial magnetic field – REF frequency, the axial magnetic field – the plasma density and the plasma density – amplitude of the applied REF voltage are shown in Figs. 11, 12 and 13, respectively. Here, β and other geometrical parameters are taken from the experimental condition and are shown in Table 2.

Table 2. Fixed parameters.

β	0.685
n_0	3.72x10^{16} m^{-3}
L	0.05 m
r_0	0.013 m
a	0.1 m

Figures 11 and 12 show that the theoretical thrust has a peak when the axial magnetic field is equal to 0.025 T. And the strength of the optimum axial magnetic field increases with increasing the plasma density. In addition, the thrust increases either by reducing REF frequency, by increasing plasma density or increasing the REF voltage.

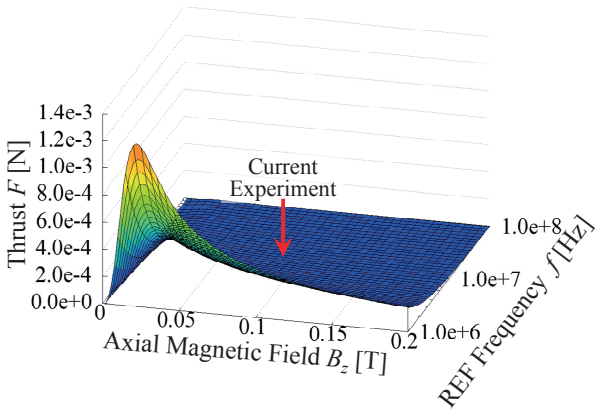

Fig. 11. Theoretical Thrust in B_Z-f Plane. Parameters plasma density n_0 = 3.72x10^{16} m^{-3} and REF voltage V_0 = 757.8 V are fixed.

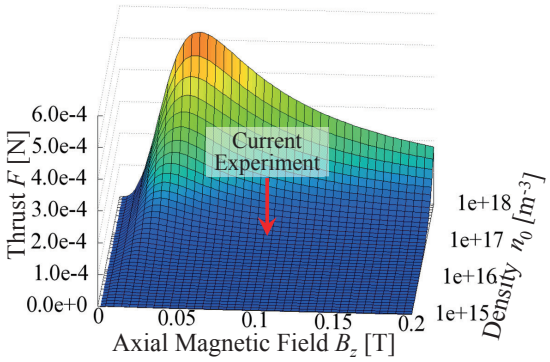

Fig. 12. Theoretical Thrust in B_Z-n_0 Plane. Parameters REF frequency f = 27.12 MHz and REF voltage V_0 = 757.8 V are fixed.

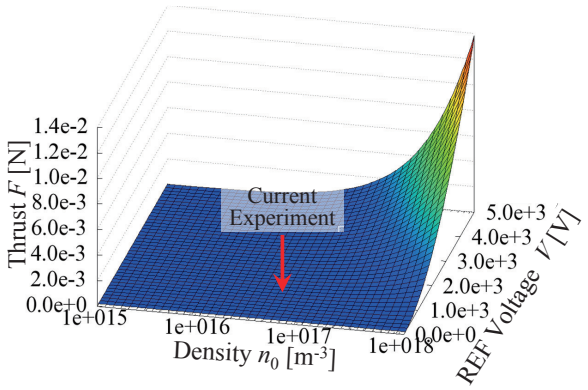

Fig. 13. Theoretical Thrust in n_0-V Plane. Parameters axial magnetic field Bz = 0.0950 T and REF frequency f = 27.12 MHz are fixed.

5. Summary

In order to realize a long-lived electric propulsion system, we have been investigating the electrodeless electromagnetic plasma thruster concept utilizing a helicon plasma source and the Lissajous plasma acceleration. We developed a laboratory model Lissajous accelerator and experiments were conducted. In the experiment, the radial profiles of plasma parameters in the plume were measured by a Mach probe. Although some features of the Lissajous acceleration were measured, most

increment of the plasma velocity is considered to be caused by the increment of the plasma temperature. A theoretical thrust model was surveyed at some parameter planes and it was implied by the survey that the thrust has a peak at an optimum axial magnetic field for the prototype. In addition, it was also implied that the thrust increases either by reducing the REF frequency, or increasing plasma density, or increasing the REF voltage from the experimental point reported in this paper.

Acknowledgments

This work was supported by the Grants-in-Aid for Scientific Research under Contract No. (S) 21226019 from the Japan Society for the Promotion of Science.

References

1) Toki, K., Shinohara, S., Tanikawa, T., Funaki, I. and Shamrai, K. P.: Preliminary Investigation of Helicon Plasma Source for Electric Propulsion Applications, IEPC-03-0168, Proceedings of the 28th International Electric Propulsion Conference, March 2003.
2) Squire, J. P., Cassady, L. D., Chang Díaz, F. R., et al.: Superconducting 200 kW VASIMR Experiment and Integrated Testing, IEPC-2009-209, The 31st International Electric Propulsion Conference, September 2009.
3) Charles, C., Alexander, P., Costa, C., et al.: Helicon Double Layer Thrusters, IECP-2005-290, IEPC-2005-156, The 29th International Electric Propulsion Conference, October 31 – November 4 2005.
4) Musso, I., Manente, M., et al.: 2D OOPIC Simulations of the Helicon Double Layer, IEPC-2007-146, The 30th International Electric Propulsion Conference, September 2007.
5) Emsellem, G. D.: Development of a High Power Electrodeless Thruster, IEPC-2005-156, The 29th International Electric Propulsion Conference, October 31 – November 4 2005.
6) Emsellem, G. D.: Experimental Investigation of Wave-Plasma Coupling on the High Power Electrodeless Plasma Thruster in Princeton University, IEPC-2009-196, The 29th International Electric Propulsion Conference, October 31 – November 4 2005.
7) Wiebold, M., Scharer, J. E. and Ren, H.: Non Invasive Measurement on the Pulsed and Steady-State, High Power MadHeX Helicon Plasma, IEPC-2009-206, The 31st International Electric Propulsion Conference, September 2009.
8) Toki, K., Shinohara, S., Tanikawa, T., Funaki I., and Shamrai, K. P.: Feasibility Study of Electrodeless Magnetoplasmadynamic Acceleration, AIAA Paper 2004-3935, The 40th AIAA/ASME/SAE/ASEE Joint Propulsion Conference & Exhibit, July 2004.
9) Shinohara, S., Hada, T., Motomura, T., et al.: Development of high-density helicon plasma sources and their applications, *Physics of Plasmas*, **16** (2009), 057104.
10) Shinohara, S.: High-Density Helicon Plasma Sources: Development and Application, I1.301, The 37th EPS Conference on Plasma Physics, June 2010.
11) Toki, K., Shinohara, S., Tanikawa, T., et al.: On the Electrodeless MPD Thruster Using a Compact Helicon Plasma Source, AIAA Paper 2008-4729, The 44th AIAA/ASIME/SAE/ASEE Joint Propulsion Conference & Exhibit, July 2008.
12) Toki, K., Shinohara, S., Tanikawa, T., et al.: A Compact Helicon Source Plasma Acceleration by RF Antennae, JAXA-RR-09-003, *JAXA Research and Development Report*, 2010.
13) Toki, K., Shinohara, S., Tanikawa, T. and Shamrai, K. P.: Small Helicon Plasma Source for Electric Propulsion, *Thin Solid Films*, **506-507** (2006), pp. 597-600.
14) Toki, K., Shinohara, S., Tanikawa, T., Hada, T., Funaki, I., Shamrai, K. P., Tanaka, Y. and Yamaguchi, A.: Plasma Acceleration in a Compact Helicon Source Using RF Antennae, *Journal of Plasma and Fusion Research*, **8** (2009), pp. 25-30.
15) Nishida, H., Shinohara, S., Tanikawa, T., et al.: Preliminary Study on Electrodeless Magneto-Plasma-Dynamic Thruster Using a Helicon Plasma Source, AIAA Paper 2010-7013, The 46th AIAA/ASME/SAE/ASEE Joint Propulsion Conference & Exhibit, July 2010.
16) Matsuoka, T., et al.: Scaling Laws of Lissajous Acceleration for Electrodeless Helicon Plasma Thruster, *Plasma and Fusion Research*, **6** (2011), 2406103-1-2406103-4.
17) Ando, A., Watanabe, T., et al.: Evaluation of Para-Perp Type Mach Probe by Using a Fast Flowing Plasma, *Journal of Plasma and Fusion Research*, **81** (2005), pp. 451-457.